Palacký University Olomouc
Faculty of Science

Department of Optics

Advanced detectors for photon counting

Master's Thesis

Jan Grygar

Palacký University Olomouc
Faculty of Science

Department of Optics

Advanced detectors for photon counting

Master's Thesis

Author:	Jan Grygar
Study programme:	B1701 Physics
Field of study:	Optics and Optoelectronics
Form of study:	Full-time
Supervisor:	Mgr. Josef Hloušek
Consultant:	RNDr. Miroslav Ježek, Ph.D.

Thesis submitted on: .....

Abstract

The detection of single photons is used in many disciplines of physics. Today, multiphoton quantum states play a key role in emerging quantum technologies. It is therefore necessary to use detectors capable of a resolution of the number of photons. This work aims to build a tunable multichannel detector capable of a resolution of the number of photons. This detector will be composed of individual avalanche diodes with quenching circuits. Therefore, in the first part of this work, I deal with the issue of avalanche photodiodes operation in the Geiger mode with passive quenching. I characterized this single-photon detector performance, such as dark count and detection efficiency dependence on temperature and bias voltage. This knowledge is used for further development of a multichannel detector. Another important part is the signal processing of the electrical output signal from the multichannel detector. I perform detailed characterization of a coincidence unit developed in our group. I also develop a library to control it. In the last part of the work, I demonstrate the use of a multiphoton detector and a coincidence unit to evaluate click statistics of light.

Keywords

`Detector, SPAD, Dark counts, Quenching circuit, Recovery time, Detection efficiency, Coincidence unit, Coincidence window, Coincidence`

Abstrakt

Detekce jednotlivých fotonů je využívána v mnoha oborech fyziky. Dnes hrají multiphotonové kvantové stavy klíčovou roli v rozvíjejících se kvantových technologií, proto je potřeba využít detektory schopné rozlišit počet fotonů. Cílem práce je sestavit vlastní multikanálový detektor, schopný rozlišit počty fotonů s nastavitelnými parametry. Tento detektor bude sestaven z jednotlivých lavinových diod se zhášecímy obdvody. Proto jsem se v části práce zabýval problematikou laviových fotodiod operujících v Geigerově režimu s pasivním zhášením. U tohoto jednofotonového detektoru jsem se zabýval parametry, jako jsou temné detekce, detekční účinnost a to v závislosti na teplotě a předpětí. Tyto poznatky slouží pro další vývoj multikanálového detektoru. Další významnou částí bylo zpracování signálu z multikanálového detektoru. K tomu jsem využil koincidenční jednotku, která byla vyvinuta v naší skupině. V práci detailně charakterizuji časové vlastnosti jednotky a popisuji mnou vytvořenou knihovnu, která slouží k nastavení parametrů a vlastnímu ovládání. V poslední části práce jsem demonstroval využití multikanálového detektoru s částečným rozlišením počtu fotonů a koincidenční jednotky k vyhodnocení detekční statistiky světla.

Klíčová slova

Detektor, SPAD, Koincidenční jednotka, Temné pulzy, Zhášecí obvod, Koincidenční okno, Koincidence, Zotavovací doby, Detekční účinnost.

Acknowledgments

First of all, I would like to express my sincere gratitude to my supervisor Mgr. Josef Hloušek and to my co-supervisor RNDr. Miroslav Ježek Ph.D. for guidance, endless patience, friendly attitude, and advice. My thanks also go to my colleagues for a friendly environment, kindness, and mutual help. Last but not least, I would like to thank my family for their care and their support.

Jan Grygar

Declaration

I hereby declare that I have written this Diploma Thesis "Advanced detectors for photon counting" and performed all the presented research and experimental tasks—by myself, while being supervised by Mgr. Josef Hloušek. I also state that every resource used is properly cited. I agree with the Thesis being used for teaching purposes and being made available at the website of the Department of Optics.

Signed in Olomouc on ....

Jan Grygar

Contents

Chapter 1

Introduction

A single-photon detector is a device capable of registration of individual electromagnetic radiation quanta-photons. The photon travels at the speed of light and interacts weakly with the environment over long distances, and photons can be manipulated with linear optics. Therefore, the single-photon detectors are expanded in a large variety applications. In quantum information science individual photons are used for encoding and manipulating information. The information is encoded in degrees of freedom of photons such as polarization, momentum, energy, etc. The quantum key distribution [1] uses single photons to establish a secret key. Another use of photons is in a quantum tomography. This is an experimental procedure to reconstruct the density matrix of an unknown quantum state. Furthermore, single photon detectors are used in applications such as light radar (LIDAR), particle sizing, gas analysis, time-resolved spectroscopy [2], nuclear and particle physics, astronomy and quantum random number generators [3, 4].

There are several detectors [5, 6] based on various physical principles for the detection of single-photon. In each case, the operating principle has advantages and disadvantages. One of the first single-photon detectors were photomultipliers [7]. The photomultipliers have very small quantum efficiency and a large noise. The other devices for detecting photons are avalanche photodiodes. The diode usually operates in Geiger mode, which provides single-photon sensitivity. Geiger mode operation means that the diode is reverse-biased above the breakdown voltage. The advantage of avalanche photodiodes is lower bias voltage and higher efficiency. The other class of detectors is based on superconducting materials. Superconducting nanowire single-photon detectors [8] offer low dark counts, short recovery times, and low timing jitter. They operate in the temperature range of 1.5–4 K below the superconducting transition temperature. The detector needs a cryostat to reach a low temperature, which is a disadvantage.

In my thesis I will focus on silicone single-photon avalanche photodiodes (SPADs). The SPAD is based on an avalanche photodiode structure (p–i–n junction) operated in Geiger mode, which needs some kind of a quenching circuit. The circuit protects the diode from a large avalanche current. Today efforts are underway to integrate quenching circuits directly with detector that improve detector parameters. The performance of the SPAD is defined by several parameters as spectral range, dead time, dark count rate, detection efficiency, timing jitter, afterpulses and recovery time. The single-photon detectors mentioned so

far are termed "binary detectors" because they can only distinguish between zero or more photons.

Nowadays, there are several ways to achieve photon-number-resolution (PNR). Detector with photon number resolution ability is superconducting transition-edge sensors (TES). The TES is a thermal sensor that measures an energy deposition by the increase of resistance of a superconducting film biased within the superconducting-to-normal transition [9]. Another way to obtain photon-number-resolution is to divide the detector active area into many small pixels [6]. Another approach is to spatially or temporally multiplex [8] non-PNR detectors. The spatial multiplexing (figure 1.1-a) is based on splitting an input optical signal by a set of beam splitters. The divided optical signal is led to multiple single-photon detectors. The time multiplex (Figure 1.1-b) is based on to splitting signals and add a delay. The signal is divided by first beam splitter 50:50. Both arms of beam splitter are recombined to form an unbalanced Mach-Zender interferometer. A relative delay in one arm is Δt. This process is repeated for other divides. This optical signal is led to binary detectors. In this case, we need only 2 detectors. The photon-number-resolving detectors (PNRD) are critically important for many optical applications and technologies such as quantum metrology [10, 11], quantum information [12, 13], and foundations of quantum mechanics [14].

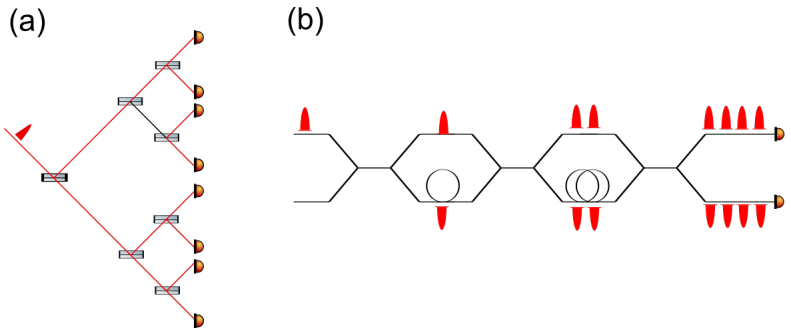

Figure 1.1: Scheme for spatial and time multiplexing of single-photon detectors.

Optical pulse with a few photons can be detected by the PNRD. Several detection events from one optical pulse detected at the same time is called coincidence. The special device for recording the coincidences is called coincidence counting unit (CCU).The coincidence unit is an important device to analyse photon entanglement, which is a basic resource for quantum communication and quantum computation. Another area of CCU use is experimental research quantum optics [15, 16], x-ray microscopy [17] and fluorescence measurements [18]. For analysis state of light is to use a PNRD with a coincidence counting unit.

The further text is structured into five main chapters. In chapter 2 I explained basic information about the single-photon detector operation. Chapter 3 describes the construction and characterization of home-built passive quenching SPAD. In chapter 4, we present a home-built coincidence counting system. The last chapter 5 is about the demonstration of the use of a coincidence unit for the analysis of light states.

Chapter 2

Avalanche photodiode

Avalanche photodiode is a semiconductor electronic device composed of a different types of semiconductors. The frequently used structure is built from a P+ layer, intrinsic layer, P region, and N+ layer. The silicon APD devices are constructed with different fabrication technology [8]. The individual constructions differ from each other in the width of the semiconductor layers. There are optimized structures that improves some parameters of a detector for a specific application. I work with a structure called shallow-junction and others are described in the books [8, 5].

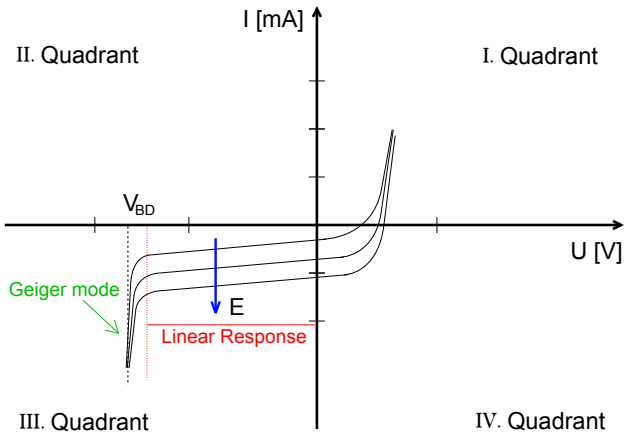

Figure 2.1: The volt-ampere characteristic of avalanche photodiode.

The behavior of an avalanche photodiode is described by a volt-ampere characteristic description in figure 2.1. The diode can operate in several modes and III. quadrant of volt-ampere characteristic is used for detection. There exist two possible operation modes. Avalanche diode works with linear response for low reverse bias voltage. This means that the response of the detector is proportional to the intensity of light as in case of a PIN diode. The diode can operate with a reverse bias voltage greater than the breakdown voltage. This kind of operation is called Geiger-mode. In this mode, the diode can detect single photons because the amplification in the Geiger-mode is non-linear. There is used

an avalanche amplification that has exponential gain. The avalanche photodiode operated in Geiger-mode with quenching circuit is called a single-photon avalanche diode (SPAD). SPAD must have a uniform voltage over the entire active junction area. The uniform voltage produces macroscopic current pulses with constant amplitude. This avoids unwanted effects such as edge effects and micro-plasmas within the active junction area.

The avalanche photodiodes are manufactured from various materials, which determine the region of the spectrum. We must use defect-free materials to ensure uniformity of carrier multiplication over the entire photosensitive area. The defect can cause afterpulses that increase noise [19]. Today, the most frequently used materials are silicon, germanium, and InGaAs.

2.1 SPAD working principle

The operating voltage V_A is applied on the diode. This voltage is bigger then the breakdown voltage V_{BD} because we used Geiger-mode. We defined overvoltage as $V_o = V_A$ - V_{BD}, and we will use this parameter for description of the voltage applied on the detector. Inside the diode is a strong electric field, but no free carrier is present. When a photon is absorbed in the intrinsic region (i), primary electron-hole pair is produced there. The carriers move towards the P layer due to the electric field. There exists a strong electric field that accelerates the carriers, and this layer is referred to as the multiplication layer [20]. Carriers that have sufficient energy excite another electron-hole pairs. This process is called impact ionization. All carriers are accelerated by an electric field and due to impact ionization, they create more carriers. This is an avalanche multiplication process. The result of the avalanche process is that each input photon may generate multiple free electrons and holes. The current then grows exponentially until reaching a macroscopic value. Now, the diode is thus switched on, and the avalanche current flows through the diode. The fast offset of the current marks the time of arrival of the photon. The device remains open until the avalanche is quenched by an external quenching circuit, which reduces the voltage below V_{BD}. When the overvoltage is reduced, the free carriers recombine. The quenching circuit then reset the voltage to the original level. In the interval when the avalanche is quenching, the detector is insensitive to any subsequent photon arriving. This interval is called dead time [8].

2.2 Quenching circuits

The SPAD needs an electronic circuit that reduces avalanche of carriers from detection event. An avalanche of carriers causes an increase in current flow, which can destroy the diode. The interruption of the avalanche current is called quenching. The quenching circuit is divided into several types such as passive, active, gate mode, and their combinations. A detailed description of the quenching circuits is discussed in [21, 22, 23].

2.2.1 Passive quenching circuits

This circuit is easy to build and allows easy measuring of SPAD parameters. Another advantage is high voltage protection for working with high overvoltage.

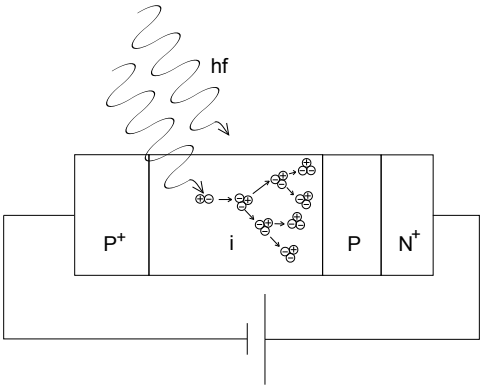

Figure 2.2: The schema of carrier pair multiplication in an avalanche photodiode.

On the other hand, the main disadvantage is the long recovery time, which significantly limits a repetition rate.

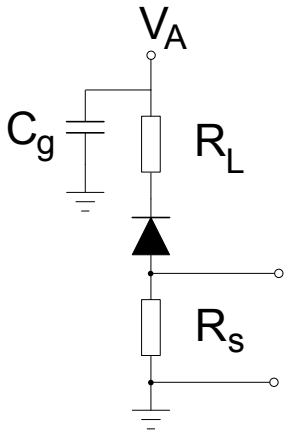

Figure 2.3: Schematic diagram of a passive quenching circuit.

The passive quenching circuit (Figure 2.3) is composed of two resistors, an avalanche diode, and a capacitor. The construction of this circuit is similar to the voltage divider. The avalanche diode is reverse biased through a ballast resistor R_L that takes away current from an avalanche. The second connected resistors R_s converts the current signal into a voltage signal. Resistor R_s serves as impedance matching. An output voltage signal of the SPAD is measured on this resistor. The last component is a capacitor C_g that is used for impedance matching also. The avalanche diode has parasitic junction capacitance C_D. This capacitance is changed by avalanche current and discharges during quenching. The diode resistance R_D is given by ohmic resistance of the neutral region and metal contactor. The circuit does two operations, quenching and resetting.

The quenching time constant T_q is set by total capacitance and by resistance R_L and R_D in parallel. Resistance R_D is quite small (about 1 $k\Omega$), and therefore

quenching time is given simply by R_D :

$$T_q = C_d \cdot \frac{R_D R_L}{R_D + R_L} \approx C_d R_D. \tag{2.1}$$

Second time constant is reset time. In this interval capacitance is slowly recharged to operation level with exponential recovery transition with a time constant T_r:

$$T_r \approx C_d R_S. \tag{2.2}$$

During the reset transition, the diode voltage is higher than V_{Bd} and an avalanche can be triggered. The voltage on the diode is lower than V_A, which means that a diode operates with lower detection efficiency. This transition is slow because the time constant dominantly depends on R_L. The pulses produced during the reset transition have smaller amplitudes.

2.2.2 Gate-quenching circuits

The circuit is designed similarly to a passive circuit. The difference is in the type of power supply. The bias voltage on the detector is the sum of the constant voltage level, lower than the SPAD breakdown voltage, and the gating signal pulse. Only when applying a gating pulse the detector is switched to Geiger mode. Outside of the gating pulse, the detector is not capable of single-photon detection. The circuit can operate in two different regimes, AC or DC coupling [22]. The gating pulse is modified by a quenching circuit, that deformed shape of gate pulse. Advantage of this circuit is low dark count rate, because the effect of dark pulse is visible only in the gate windows. The main advantage is high speed of quenching process allowing ultra-high repetition rate.

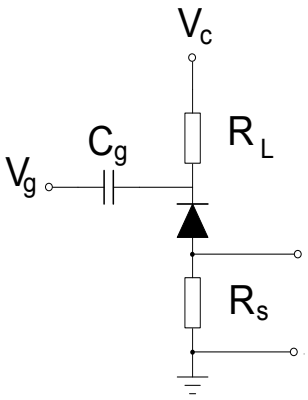

Figure 2.4: Schematic diagram of a gate-quenching circuit.

We focus on AC coupling (Figure. 2.4), where a pulse generator is connected via a capacitor C_g to a passive quenching circuit. This connection creates a differentiator filter that is made by a capacitance and ballast resistors R_l . The differentiator filter has a negative effect on the amplitude and shape of the gate pulse. The true amplitude V_A on the detector is attenuated by differentiator

filter. The shape of the gate pulse is deformed, because the filter cut-off high frequencies. The discharge of the filter causes that gate pulse to have a long negative tail. This negative tail corresponds to slow-release capacity C_g in a gate off-time T_g. The negative tails from all gate pulses are cumulated in linear superposition and build a baseline offset of constant voltage. For proper operation, it is assumed that only one detection can occur during a gate pulse. Upon detection, the circuit behaves like a passive quenching circuit because it has long recovery time. The quenching is accelerated by a voltage drop after the end of the gate pulse.

2.2.3 Active quenching circuits

This technique avoids the disadvantages of a passive quenching circuit such as long recovery time. The basic idea is to quickly detect an avalanche and restore the detection efficiency back to the operational level by controlling the a bias voltage source. This active quenching circuit (ACQ) was devised by Cova [24].

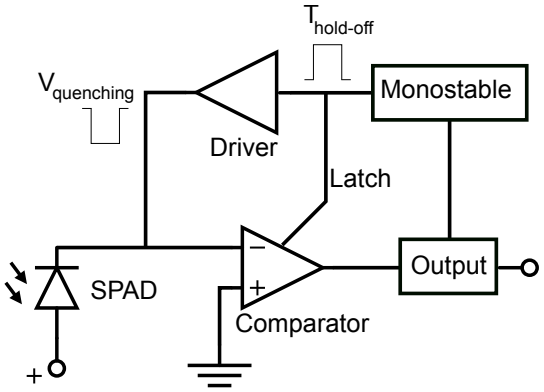

Figure 2.5: Schematic diagram of an active-quenching circuit.

The operation of this circuit is: The rise of avalanche is sensed by a fast comparator that switches the bias voltage source below breakdown voltage (quenching time). After the exactly defined hold-off time the bias voltage is switched back to operation level. The time required for voltage recovery is called the reset time. The processes of quenching and resetting are carried out using active components that are pulse generator or a fast switch. A basic diagram of AQC is presented in the figure 2.5 .

The photon absorbed in the diode triggers an avalanche. AQC detect avalanche and starts quenching procedure. Before active quenching begins, passive quenching takes place (Figure 2.8). The time required for detection depends on the sensitivity of comparator and the peak value of avalanche current. If the quenching process starts too late the total avalanche current can destroy the diode. On the other hand, the time before quenching must be long enough for the comparator to detect an avalanche. These two conditions limit the quenching time T_q. After quenching time, the hold-off time starts. The hold-off time is the time in which the free electron-hole pairs recombine and the afterpulses decay. The length of the hold-off must eliminate the main part of the probability of afterpulsing due to trapped carriers. The last part to restore the

detection efficiency is reset time. During the reset time, the voltage is increased to the operating level. The reset time has usually only a few nanoseconds and dependent on the overvoltage and parasitic capacitance of a diode. The sum of all these time interval (quenching, hold-off, and reset) gives a recovery time. The recovery time of AQC is much faster than the PQC, but it cannot be infinitesimally small as we explained above.

The design of the AQC has some problems. The major problem is the high difference between the amplitude of the avalanche pulse and the quenched pulse. The comparator is triggered by the avalanche pulse, which has only a few millivolts, but quenching pulse has amplitude about volts. The comparator can be retriggered by the reflection of the quenching pulse and AQC would start oscillating. This problem increases the number of afterpulses.

2.2.4 Mixed quenching circuits

Another type of quenching circuit combines active and passive technics. These circuits overcome the limits of purely passive and active quenching circuits because this approach takes advantage of both circuits. The most used class is active-passive quenching with active reset [25] . This kind of quenching circuits is constructed that avalanche diode is connected both to ballast resistors and to active reset circuit. Many classes of quenching circuits exist in this category [23, 21].

2.3 Processing of electrical signal from SPAD

The output of the passive quenching circuit are electronic pulses. The pulses have different amplitudes, which can differ by 100 % amplitude. Further, it is caused by afterpulses which retrigger new avalanche. The reason of different amplitude is slow increasing of detection efficiency to the operation level. This is typical problem for passive quenching when detecting a continuous optical signal. The problem is solved by monitoring the output from the detector after time T_m called electronic recovery time. This time is selected based on the reset time and is usually fivefold of reset time $5T_r$. After time T_m the voltage on detector is almost at the operational level. The comparator is employed for sensing avalanches, pulses smaller than the threshold level are discarded, producing a dead time that is neither well known nor stable [8]. The signal from a comparator is then processed by pulse shaper, that usually produces TTL pulses. Active quenching circuit has very short reset time therefore it does not have this problem. The active quenching circuit has a well-defined recovery time. The output electronic pulse is processed in the same way as for a passive quenching circuit.

The output of SPAD can be processed in many ways. One option is to count the detection rate. The device for the counting number of detection events is called counter. The basic principle is: if the amplitude of the pulse is greater than the counter threshold, the event is recorded. To characterize time performance time-to-digital (Time Tag) [26] converters are used. Time tag devices record timing events and provide a timestamps. This device is used to measure the time characteristics of detectors such as dead time. Furthermore, the device can be used for time-correlated single photon counting (TCSPC).

Coincidence units are used to record coincidences. These devices can be used to study statistics of light, for example.

2.4 SPAD parameters

In this section we present basic parameters of SPAD. The characterization of detectors is fundamental for description of devices such as single-photon sources [27]. SPAD is characterized by several parameters [8]. Individual parameters are important in different applications.

Efficiency
The photon detection efficiency describes the probability of conversion of photon to an output signal. Quantum efficiency describes only conversion of photon to primary pair electron-hole. This value is bigger than the photon detection efficiency. The photon detection efficiency increases with excess bias voltage because the electric field in active volume is stronger. This gives the carriers greater acceleration, and it increases multiplication. Detection efficiency increases linearly at a low excess voltage. At high excess voltage, the detection efficiency is saturated. Detector with thick-junction has higher efficiency than a thin-junction detector because the absorption has an exponential dependence on length of absorption region .

Timing jitter
Timing jitter (Figure 2.6) is the width of full-width at half maximum (FWHM) of photon detection time distribution. Jitter is composed of two components. The narrow peak is due to carries photo-generated in the junction depletion layer. The carriers in this layer are immediately accreted by the electric field. The second component is slow tail due to photo-generated in intrinsic region, which is near to depletion layer. Carries in the junction depletion layer moves by drift velocity that is faster than the diffuse velocity in the intrinsic region. The photo resolution is limited by a slow tail. The amplitude and duration of the tail depend on wavelength. This is a limitation for applications where the light source is not monochromatic. The diffusion includes two main effects: multiplication-assisted lateral diffusion of carriers and photon emission from hot carriers in an avalanche. The narrow peak and slow tail are improved by higher electric field is caused by increasing the overvoltage.

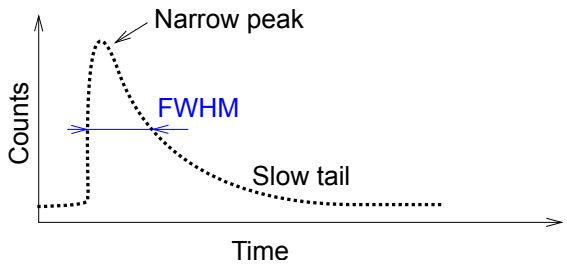

Figure 2.6: Typical time resolution (jitter) of arrival photon.

In the context of the SPAD multichannel detector, it is important to reduce

the timing jitter. The timing jitter limits the width of coincidence windows. The better defined event time provides smaller coincidence window.

Dark counts

Dark counts are one of the noise source of SPAD. This is a similar effect as dark current in ordinary photodiodes. Dark counts are carries thermally generated within the SPAD junction. This effect is present in the absence of illumination and works during the operation of the detector. Dark counts have the Poissonian fluctuation. Dark count rate increases with overvoltage. The rate increase is caused by effects of fields-assisted enhancement of emission rate from generation center, increase of avalanche triggering probability and bant-to-band tunneling. Avalanche triggering probability is related to an increase in detection efficiency. High field intensity causes band-to-band tunneling, which significantly contributes to DC. Tunnel-assisted generation cannot be reduced by lowering the temperature and therefore sets a limit to the reduction of DC.

Also, dark count rate increases with temperature also. The kinetic energies of the carriers increase with temperature, and carriers are easier to releases into the conduction band. This effect causes a strong generation of free carriers that triggers an avalanche. The quality of material and technological helps reduce dark counts.

Afterpulses

The afterpulses are another source of the noise. The carriers from avalanche are captured into intermediated energetic levels of impurity and defect. The lifetime of trapping carries is statistical; the emission probability is the negative exponential time constant for each involved level. The released carriers can retrigger further avalanche, which is not caused by a photon. It can be seen from the statistics that most afterpulses are immediately after the recovery time. For a quenching circuit, with short recovery time, afterpulses significantly increase noise. Low temperature causes more afterpulses because lifetime is longer. Trapping carriers need energy from temperature fluctuation to release from trapping centres.

Recovery time

Recovery time (Figure 2.7) is the time interval during which the detector cannot register photon. The recovery time is divided into dead time and reset time. The dead time follows the absorption of a photon and in this interval the detection efficiency is zero. In the reset time the excess voltage raises to operation level. In this interval photons can be registered, because detection efficiency is non zero. The detector in this interval is undesirable. The recovery time limits the maximum count rate of the detector. The factors influencing recovery time depend strongly on the type of quenching. Recovery time in an active quenching circuit (Figure 2.8) is deliberately lengthened to suppress afterpulsing.

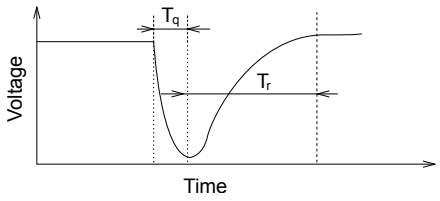

Figure 2.7: The waveform of recovery time for passive quenching circuit.

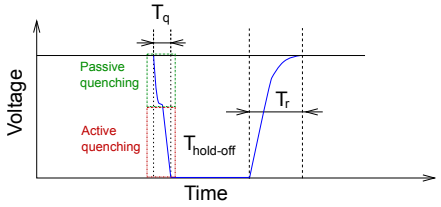

Figure 2.8: The waveform of recovery time for active quenching circuit [28].

Chapter 3

Characterization of passively quenched SPAD

Here we introduce a home-build SPAD. The main building block of this detector is the avalanche photodiode SAP500. The quenching is assured by the passive quenching circuit. We study the parameters of this SPAD. Our results will be used for a development multi-channel detector with an adjustable parameters.

3.1 The SAP500 - the comercial silicon APD

For our the passively quenched SPAD, we used an avalanche photodiode (APD, SAP500) manufactured by Laser Components [29]. The construction of the diode supports operation at room temperature and provides single-photon detection. The diode can operate at a temperature range from -40 up to 85 °C. This APD is sensitive in the range of 400 nm to 1100 nm, and the sensitive peak is at 700 nm. The active area is circular with a diameter of 500 μm. The conversion region is 25 μm wide and situated between the p+ layer and the p region. The shorter conversion region helps to reduce timing jitter of the photon-photoelectron conversion and allows operation at the low breakdown voltage. SAP500 has a breakdown voltage of approximately 125 V. To increase quantum efficiency, the junction layer is covered with a metal layer that works as a mirror. The entrance surface is covered by a broad-band AR coating for minimization of reflectance. This APD is coupled to a multimode fiber with numerical aperture 0.2. The parasitic capacitance of a diode is typically 3.3 pF. This parameter is important for a design of the quenching circuit. The diode is hermetically sealed in the metal case TO-46 without built-in Peltier element.

Parameters of SAP500 significantly depend on the temperature, therefore we used external Peltier cell (Thorlabs, TECF1S). Peltier cell can cool the detector down to -10 and warm up to 50 °C. Thermistor (TDK, B5755161103F) is connected to a detector and Peltier cell with heat-conducting tape. This system is closed in the box for better temperature stability. The box also contains a silica gel to avoid condensation of water. Water may cause a short circuit and destroy the detector. To block the water condensation, we need to cool the detector slowly only a 3 degrees per minute. Temperature is monitoring by a thermistor connected to the temperature controller (Thorlabs, TED4015) with

adjustable PID parameters.

We used a passive quenching (see chapter 2) as shown in the figure 2.3. The circuit contains two resistors R_l=560 kΩ and R_s=220 Ω and capacitor C_D = 100 nF. From the theory, we estimate the quenching time for this circuit (given by the formula 2.1) equal to $T_q \approx 3.3$ ns and the reset time (given by the formula 2.3) is $T_r \approx 1.85\mu$s. These times provide the range in which the dead time T_D is localize.

3.2 Experimental setup

In this subsection, we describe the experimental setup used for characterization of the detector. The scheme of the whole experimental setup is presented in Figure 3.1. The experimental setup is composed of signal preparation, measured detector, and electrical signal processing from the detector. The signal preparation is divided into two regimes, which differ in the optical source.

First, I describe how to implement the pulse regime (Figure 3.1). Pulsed light is generated by gain-switched VCSEL diode driven by electronic pulse generator with a repetition rate of 750 kHz; the pulse length is 1 ns. The VCSEL is emitting a pulse of light at a central wavelength of 810 ± 10 nm. The light pulses are led to the attenuator by a multimode fiber. The attenuator is composed of the neutral density (ND) filters. Then the signal is led to the detector by a multimode fiber. We use a reference detector RF (Excelitas SPCM CD 3432 H, S:24334) to calibrate the optical source. The detection rate on RF was set to 50 kHz. This rate is a trade-off between the signal to noise rate and a convenient single proton fraction. We require a signal to noise rate greater than two. The DC for SAP500 is up to 25 kHz, therefore the detection rate on RF is 50 kHz. The ration between the electronic pump signal and the optical signal is small (≈ 0.07), therefore the optical pulse contained only one photon with high probability.

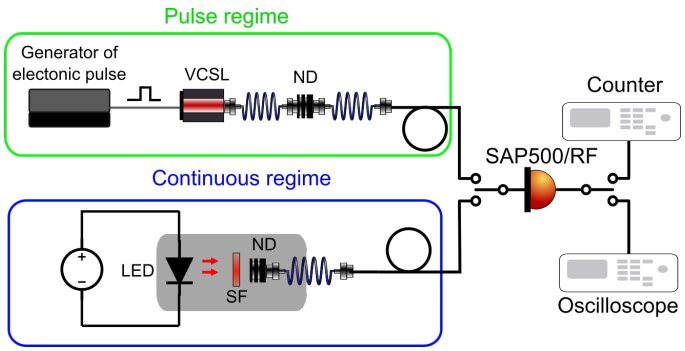

Figure 3.1: The setup for the characterization of home-made SPAD. The setup has two configurations: pulse regime and continual regime. The continuous regime uses LED as an optical source. The optical signal is filtered by the narrowband spectral filter and attenuated by ND filters. The pulse regime uses VCSL diode driven by the generator of an electronic pulse. The optical signals are both attenuated by ND filters and led to the detector. The output of the detector is measured by oscilloscope or counter

The continuous regime (Figure 3.1) is created by LED (MarkTech, MTE2081-OH5) illuminates with a wide spectrum that have FWHM 40 nm. The LED is driven by laboratory source (Aim TTi, OL355T). The optical signal is led via free space to spectral filters and ND filters and coupled to multimode fiber. We used narrowband spectral filter for selection wavelength 810 nm. This optical signal is led to the detector. The detection rate of the reference detector was set to 70 kHz. The detection rate is set by the same criteria as in the case of pulse regime.

The detector is connected to adjustable laboratory power supply (TDK lambda, Z650-0.32) that provides voltage from 100 to 200 V. This source is used to adjust the voltage on the detector, which allows us to measure the dependence of detector parameters on the voltage. We also control the temperature by the temperature controller. This controller allows to set the temperature from -55 to 150 °C with a resolution of 0.001 °C.The output of the detector is led by BNC cable to an oscilloscope(LeCroy, wavepro 7ZI) or a digital counter (VTPUP, Countex).

3.3 Dark count

We characterized the dark count rate dependence on the temperature and overvoltage. The detector starts producing dark count at breakdown voltage, 126.4 V(25 °C) for used detector (SAP500, s.n. 00094B001). We choose 6 values of temperature in range -5 °C to 25 °C and 10 values of overvoltage from 0 V to 30 V. The output of the detector is monitored by the oscilloscope. We characterized the output pulse parameters of our detector. The amplitude of each DC is not the same (see chapter 2.2) and this variability leads to the problem of setting an optimal threshold of the counting system. We measured the dark pulses on an oscilloscope by waveform acquisition of amplitude(Figure 3.2). We recorded amplitudes for different overvoltages and temperatures. The average value of the amplitude of dark pulses for 0 °C and 2 V is 0.20(6) V and mode is 0.26 V, where the mode is the value that appears most often in data set. For 0 °C and 18 V is average amplitude of DC 0.7(2) V and mods is 0.56 V. For 10 °C and 2 V is average amplitude of DC 0.1(1) V and mods is 0.11 V and for 10 °C and 18 V is average amplitude of DC 0.6(2) V and mods is 0.72 V. We can see that the amplitude of DC grows with overvoltage (Figure 3.2a). On the other hand DC amplitude decreases with increasing temperature (Figure 3.2a). From waveform acquisition of amplitude we find the smallest amplitude of the dark pulses. The trigger level for the counting system (Countex) is set to capture even the smallest amplitude of dark count. This procedure we repeat for each set of measurements. We found that the rate of DC grows up with overvoltage and temperature. This is assumed behaviour (Figure 3.3).

3.4 Relative efficiency

The dependence of relative detection efficiency on temperature and overvoltage was measured in the pulsed regime. First, we measured DC and the number of optical detection for a reference detector (RF). For the true rate of the incoming photon, we subtract the number of DC from the optical detections. This value

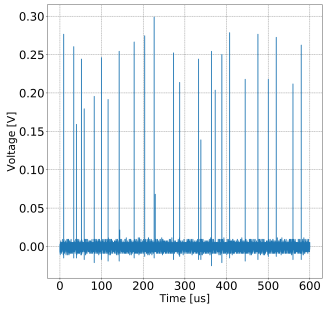

(a) V_o = 2 V and T= 0 °C

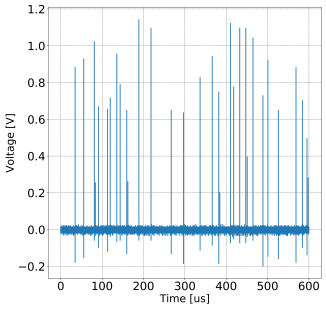

(b) V_o= 18 V and temperature 0 °C

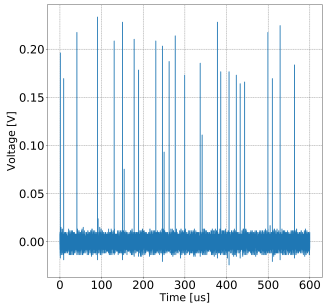

(c) V_o= 2 V and temperature 10 °C

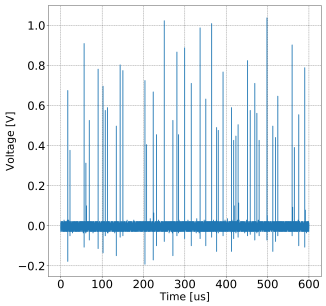

(d) V_o= 18 V and temperature 10 °C

Figure 3.2: Dependence of DC amplitude on overvoltage and temperature.

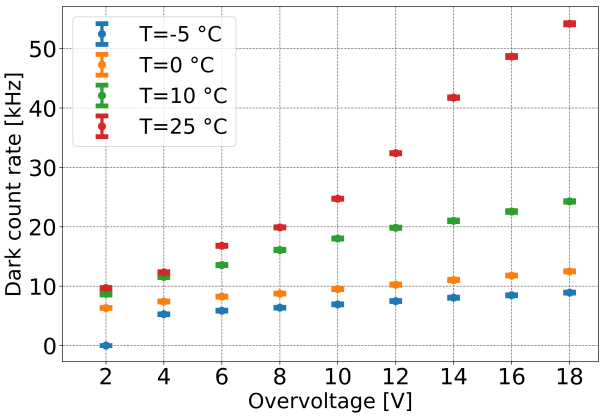

Figure 3.3: DC rate as a function of temperature and overvoltage. With increasing temperature and overvoltage, the number of dark pulses increases.

of incoming photons serves as the norm for our SPAD.

We tested dependence of efficiency on temperature and overvoltage. We chose two temperatures 0 and 15 $°C$ and overvoltage from 2 up to 20 V. Each measurement contains two parts, the first is a DC measurement and the second is an optical signal measurement. The DC is measured and serves mainly for compensation. The optical signal has a similar behaviour as DC, therefore we use waveform acquisition of amplitude on the oscilloscope (see chapter 2). The record from the oscilloscope includes two data array, one is an output of SAP500, and the second is a trigger from the pulse generator. These data are recalculated on a computer to a detection rate. The recalculation is performed using a function to find the locations and the value of the detection peaks. Trigger record can almost completely eliminate DC because of response on an optical signal is immediately after trigger. Trigger signal announces measurement on time windows that can be joint in a histogram of detection event.

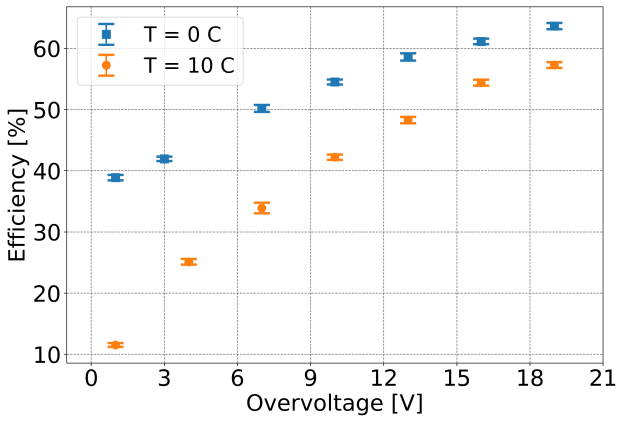

Figure 3.4: The dependence of photon detector efficiency on overvoltage for two temperatures. Axis Y is recalculated by overall efficiency for the reference detector.

The figure 3.4 shows the dependence of the relative detection efficiency on overvoltage and temperature. We compared the measured rate on the SAP500 and the reference detector. Reference detector has detection efficiency 66% according to datasheet. According to the rate of the reference detector, we re-calculated the detection efficiency for our SAP. For both temperatures, detection efficiency increases with overvoltage. The higher efficiency is reached for lower temperatures. For 20 V of overvoltage and T=0 °C the detection efficiency of SAP500 approaches the reference commercial SPAD.

3.5 Dead time

We also tested a detector SAP500 with a continuous signal. We record the waveform of optical detection from an oscilloscope and process a histogram of a spacing between pulse of detector (Figure 3.5). The histogram (Figure 3.5) shows dead time of SAP. Detector manufacturers use different methods to

evaluate dead time [30]. I use a time interval up to half the leading edge of the detected pulses (Figure 3.5). The most of detection is immediately after dead time and these detectings are called after pulses. We used a passive quenching circuit and therefore the detections after dead time have small amplitudes (see Chapter 2.2). Histogram of the spacing of detection events shows that the dead time T_D of SAP500 is not constant but changes with overvoltage. The difference is due to a slope of increase of detection efficiency after detection. At higher voltages, the detection efficiency increases faster. Another cause is parasitic capacitance of quenching circuit. The detector is also connected to the quenching circuit by long cables which also has parasitic capacity. In the next version, these shortcomings will be eliminated by better circuit design and the use of SMA resistors.

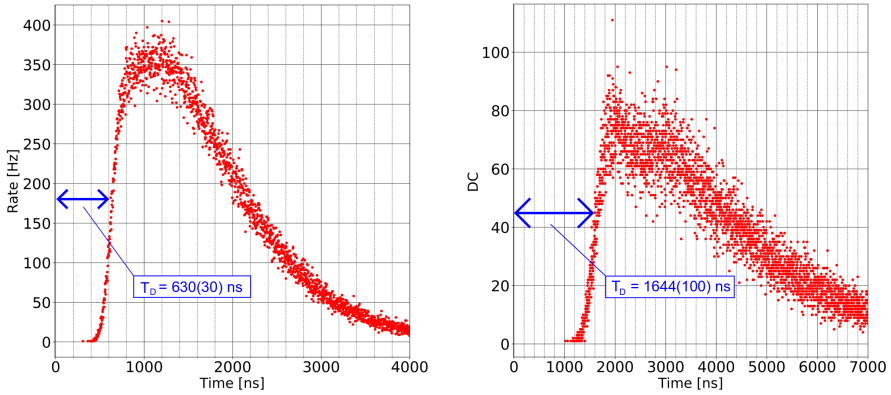

(a) Dead time for overvoltage of 20V. (b) Dead time for overvoltage of 4 V.

Figure 3.5: Histogram of spacing between pulses for temperature $10°C$.

We can compare recovery time of commercial passive quenching detector (ID-Quantique ID 120.500-800) with SAP500. For SAP500 we measure only dead time and we can see that the dead time of SAP500 is longer than the recovery time of a commercial detector passively quenched detector. The commercial detector also has stable recovery time according to the datasheet, unlike our detector. The second commercial detector has active quenching (Excelitas SPCM-CD 3605 H). We can se a very big difference in recovery time.

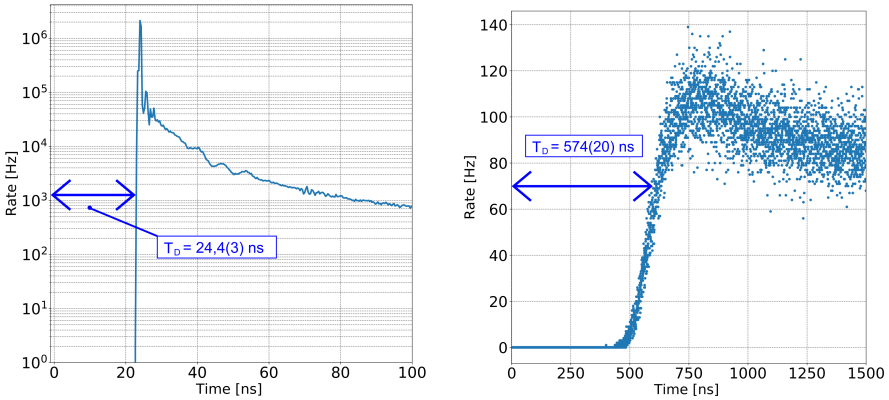

(a) Excelitas SPCM-CD 3605 H .[31] (b) ID-Quantique ID 120.500-800. [31] x

Figure 3.6: The recovery time for commercial detector.

Chapter 4

Home-built coincidence counting system

In this section, we present fast multichannel coincidence counting unit (CCU) developed in our group. My goal here is to review its working principles and perform its detailed characterization. This device works in real-time and contains 16 independent channels. Coincidence event has been defined as simultaneous detection of two or more signals from different detectors. The CCU is frequently used in various applications as quantum communication [32], quantum computation [33], quantum simulations [34] and fluorescence measurements [18].

4.1 Realization

Our system is composed of 9 circuit boards the main board and eighth doughtier boards. The mainboard contains a micro-controller (MCU, STM32F429) and the components for signal synchronization, settings, and signal processing. Each doughtier boards contains each two individual channels, voltage sensors, and temperature controller.

The whole circuit is built with ECL logic due to fast transition times enabling precise time resolution 9 ps in average. Each channel is composed by shaper and latche (Figure 4.2-a). Shaper (Figure 4.1) is a key circuit building block consists of a fast comparator (Dual ECL Ultra-High-Speed Comparator MAX 9600), bistable multivibrator termed flip-flop (MC100EP51), system of two parallel delay lines (MC100EP195 ECL Programmable Delay Chip), and basic logic gates (MC100EP05 ECL 2-Input Differential AND). Adjustable delay lines (each has 1024 step) allow precise setting of coincidence windows and compensating time misalignment of channels and other timing errors originated in an experiment. The input comparator sets the threshold in range -1 V to 4 V. The signal that is larger than the threshold and has a sufficient slope can be registered. The condition of a slope is named overdrive. The signal from the comparator is led to flip-flop. This circuit produce pulse for the delay line. The key component of the latch is the logic gate AND (MC100EP05 ECL 2-Input Differential AND). The gate compares overlay of channel windows and trigger windows. If windows have an overlay, Latch sends logic bite to MCU.

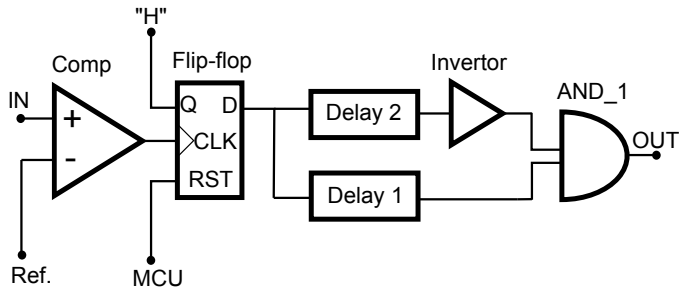

Figure 4.1: A block diagram of a shaper.

MCU controls all parts of CCU and contains a list of basic commands. The coincidence unit is connected to computer by USB cable and communication provided by serial port. The connection has a baud rate set on value 921600, and we used the RTC+CTS protocol. MCU sends an answer after every command for control. The answer is two-bite messages where zero means the successful execution of the command. Value 256 means that a command is not executed. These characters represent the Unicode code. MCU also accumulates a histogram of coincidence events. We can choose two types of histograms. The full histogram contains complete information about all coincidence events with the channel number resolution. All combinations of 16 channels give 65536 kinds of coincidence events. This number includes singles and no-detection events, for whom it is reserved 4 bytes in memory because of their higher probability of occurrence in general. Singles are an event where only single detector clicked. Singles can be described as a coincidence between a trigger and one channel. Other coincidences (means two-fold and higher) are saved as 2 bytes in MCU memory. The channel that shares in the coincidence present the position in the histogram. For example, three-fold of channels 1,4 and 6 is labelled as "0000000001010010". The same coincidences are stored in a defined position in MCU memory. The duration of data acquisition is limited by the recording rate of storage. This process requires about 0.05 s. Memory overflows if the number of high fold coincidences is higher than 65536. This problem can be solved by setting the frequency of reading properly so that the memory cannot overflow. The second type of histogram contains the sum of individual orders of coincidences. Every order of coincidences have reserved 4 bytes in memory. It means that the size of these histograms is only 68 bytes and transfer to PC is very fast. The time of data transfer from CCU to PC is only 0.1 s for a reduced histogram and 0.9 s for a full histogram. The maximum processing rate is about 3M events for the reduced histogram and 2M events for the full histogram. The difference in processing frequency between types of histograms is caused by data processing in MCU. At last, reset prepares a channel for a new measurement.

Here, I describe the signal processing depicted in figure 4.2-b. The signal comes to the channel, and if the amplitude of this signal is larger than the threshold, the comparator (comp) generates a pulse. The comparator registers only rise edge. The pulse from (flip-flop 1) starts the time axis of the channel from which the delay line is set. Now the delay lines will start to be set according

to the setting. The first is set delay1, which defines the start of channel windows. After that the delay 2 is set and negation is applied. The value of delay1 must be smaller than the value of delay2. The negated delay 2 defines the end of channel windows. These two signal edges are evaluated in logic gate AND1. The same procedure creates a window for the trigger. Both windows are processed in logic gate AND2. Component AND2 evaluates whether the windows overlap is sufficient. If the window overlay is sufficient, the latch generates a logical 1 and sends it to the MCU. The histogram is accumulated in the MCU.

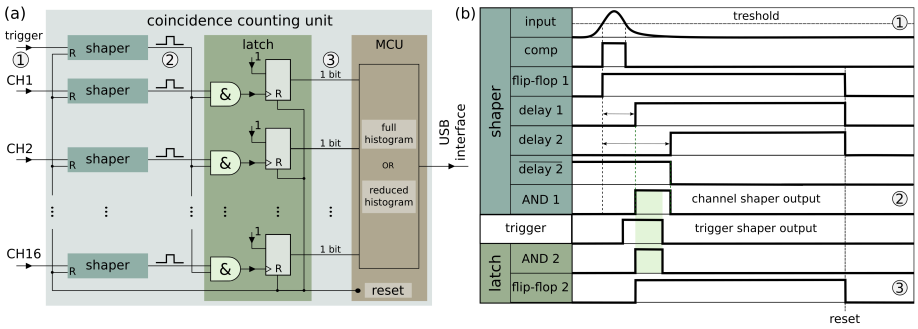

Figure 4.2: (a) A block diagram of a coincidence unit, and (b) description of the signals processing.

The coincidence counting system contains some imperfections. One of the imperfections is the non-rectangular shape of the window on the channel and the trigger. In our case, the coincidence window is defined as an overlap integral of channel and trigger windows. The non-rectangular shape of channel or trigger windows caused that the coincidence window is also deformed. Another imperfection is induced by trigger window distribution. The trigger window is distributed to all channels using repeaters which deform its waveform. The described imperfection cause blurring of the edges. In the future version of CCU will be new method of trigger distribution free of this type of error. Another problem is temperature stability. The monitoring temperature is important for stable measurement because the range of delay lines is dependent on temperature. Temperature increase causes extension of the delay line step and constant offset. The fluctuating temperature can destroy window alignment when measuring coincidence. Stabilization is provided by two 140 mm Pc fans. Temperature sensors indicate a temperature fluctuationwith accuracy of $3°C$. The exact temperature dependence of the delay line cannot be measured, therefore the effect of temperature fluctuation worsens the parameters of the unit and we cannot compensate for it. Every electronic equipment needs specific operation voltage for the right work, therefore we monitoring voltage by sensors. If the voltage is below the operation level of the equipment, channels work unstably. The sensors are intended primarily for monitoring and do not serve to compensate the monitored parameter.

4.2 Software

The CCU needs software for correct functionality. I wrote a library for the precise operation of the coincidence unit. I used the Python programming language to write the library. CCU is controlled via commands from the PC via the USB interface. This library includes functions that ensure user-friendly operation. These functions are composed from basic commands from MCU (see Appendix A) and allow easy operation. The functions send a command to MCU and interpret answers. An answer comes after each command and contains 4 Unicode code characters, which are stored in a buffer. The interpretation of the data depends on the correct synchronization. Synchronization guarantees that command with correct parameters is executed. If answer is not read all, some character stays in the buffer and destroy synchronization. The function of my library are describe in appendix B.

4.3 Coincidence unit performance

We characterize the shape of coincidence windows and consistence of n-fold coincidence probability. For this calibration, we developed a generator of pulses (PULSER) with 16 channels. Each channel has an adjustable delay with range 10 ns. The PULSER has an amplitude of 2.26(1) V and length 49.5 ns (see Figure 4.3). The signal is generated by simple relaxation oscillator whose output is delayed by RC low pass network and fast inverter with Schmitt trigger inputs (74ACT14T). The shape of pulse simulates output from the SPAD detector. The parameters of the pulse are measured on an oscilloscope(LeCroy, wavepro 7zi). The rising edge from 20 to 80 % is 580(20) ps (Fig 4.3) . The repetition rate can be chosen from 200 kHz to 10 MHz. We used frequency 506.6(1) kHz. This frequency is the same for all channels, and the individual channels do not fluctuate with each other in frequency.

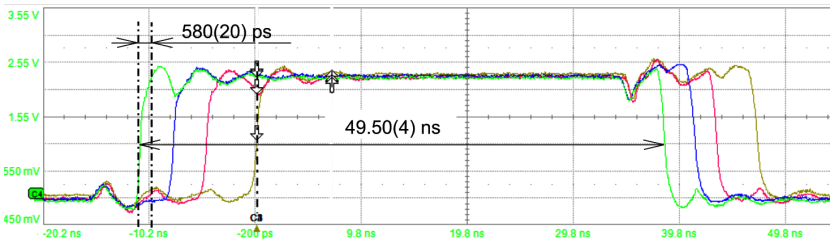

Figure 4.3: The rising edge of electronic pulse from 16-pulses generator.

4.3.1 Princip of scanning

I created a method for scanning the channel. The method is self-scanning because scanning is using the device itself. The process has two parts termed a coarse scan and fine scan. The principle of operation is: the trigger is fixed in a defined position and channel window is scanned across the trigger.

For using a scan, we must have enough space before and after channel windows. This condition limits the size of coincidence windows to 7 ns for this

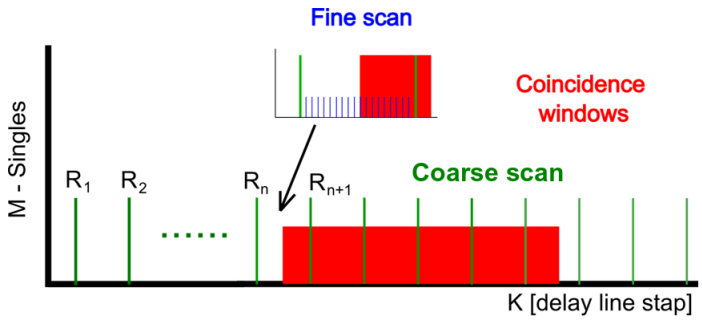

Figure 4.4: Principle of the coarse and fine method of coincidence window scanning.

method. To be able to measure these coincidence windows, we will use a variable window on the channel. Variable windows mean that length of windows is contracted after measurement of a rising edge of coincidence windows. The falling edge of coincidence windows is defined only by the falling edge of the trigger pulse, and does not depend on the length of the channel windows. It allows to reduce the length of the channel window. The coarse scan operates as: The range of delay lines is divided by a quarter of the sum of the window and trigger width. This defines the points $R_1, R_2, ...R_n, ...$ Singles are measured at points $R_1, R_2, ...R_n, ...$ (Fig. 4.4). In the point R_{n+1} we measure first singles. Now we know where the coincidence window is localized, and we use fine scanning (fig. 4.4). Fine scanning starts one step before coincidence window (R_n). The coincidence window is measured by one step of the delay line (9 ps). Scanning ends when the singles drop to zero and remain there for 10 steps. This procedure takes a long time, but we measure the whole shape of the coincidence window.

The bigger coincidence windows must be measured by the external PULSER with adjustable delay. The variable channel window is used to measure the maximum coincidence window.

4.3.2 Coincidence windows

For the testing shape of coincidence windows, we used our 16 pulse generator. The signal from the generator is carried to the channel input. We analyse the shape of coincidence windows: rising edge, falling edge, and width. For this measurement, we used the scanning of channels by function calibration. We set channel and trigger windows to the same width. To demonstrate the functionality of the CCU, we chose three channels at random. These three channels represent typical channels. We measure the characteristics of these channels for different width of coincidence windows (400ps, 1ns, 2ns, 3ns, 4ns, 5ns). The width of the coincidence window is calculated from half of the rising edge to half of the falling edge. The shape of one channel is measured 100 times. In each measurement, we evaluate the length of rising and falling edges. The following figure illustrates channels with the best edge (4.5a) and typical edge length (4.5b).

We find that length of both edges is not constant but fluctuates at the time and with the values of the set parameters. The average value of the rising edge

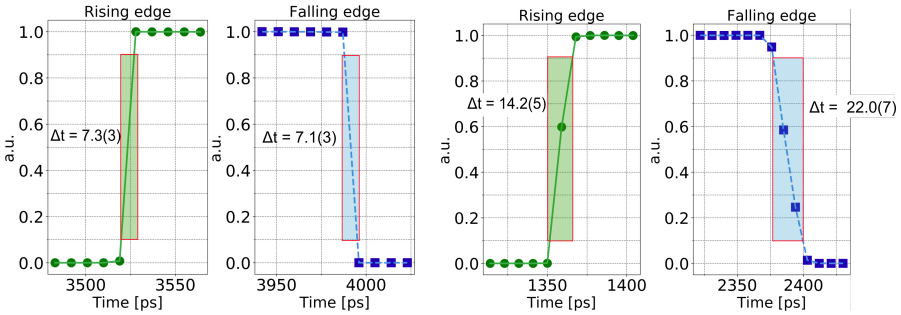

(a) The rising and falling edge for channel 7.

(b) The rising and falling edge for channel 5.

Figure 4.5: Steepness of the coincidence window edge for different coincidence windows. The edges are evaluated from 10 to 90 %.

is 15(3) ps, and the average value of the falling edge is 22(9). The best achievable edge has only one step of the delay line (9 ps), it corresponds to the length (10-90%) $\approx$ 7 ps. These edge length was measured for several channels. The smallest measured coincidence window is 400 ps. The smallest coincidence window cannot be set for all channels, because some channel has worse parameters of delay line. We confirmed that length of both edges is negligible compared to the length of the coincidence window, and coincidence windows are rectangular. In all cases the length of edge is smaller than 0.3 % of the total width of coincidence windows.

4.3.3 Higher-order coincidence efficiency

To measure the stability of the coincidence-fold, we must set all windows to the same length and must be aligned. The function **Set_width** set the same length for all coincidence window and align them (fig 4.6). This function has an alignment set with a deviation of 30 ps. This deviation is because the process of stretching and shortening windows is iterative. Due to the deviation, the length of the coincidence window converts to the required value. The deviation also compensates fluctuation of the length of coincidence windows due to temperature fluctuation.

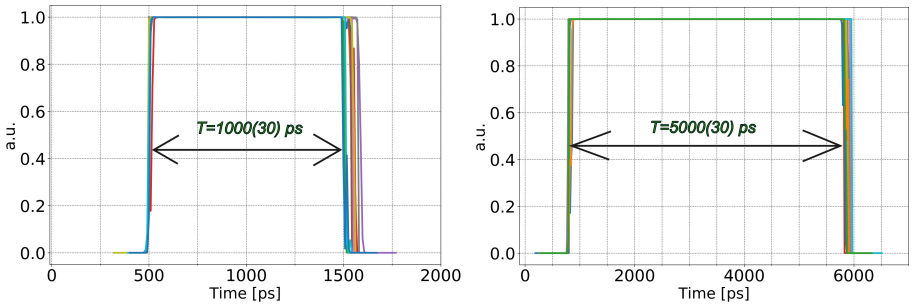

(a) Coincidence windows 1 ns.

(b) Coincidence windows 5 ns.

Figure 4.6: Alignment of coincidence windows by function set_width().

We made a measurement up to 16-fold coincidences. We measured 10 different combinations of gradual switching on of individual channel. We measure every combination of channels 100 times and each measurement lasted 0.1 s. We evaluated statistics error from the measured data. The figure 4.7 shows a measurement of coincidence windows that is 3 ns and 20 ns long. We can see that differences between individuals order is 0.18 % for 3 ns coincidence windows and 0.15 % for 20 ns coincidence windows. We also measured 2 ns and 5 ns coincidence windows with the similar result. We see that the coincidence-fold stability is very high. From all the measurements performed we can say that the fluctuation of coincidence-fold stability is up to 0.2%. The great advantage of this unit is that it has the same fluctuations for single and for 16 coincidences.

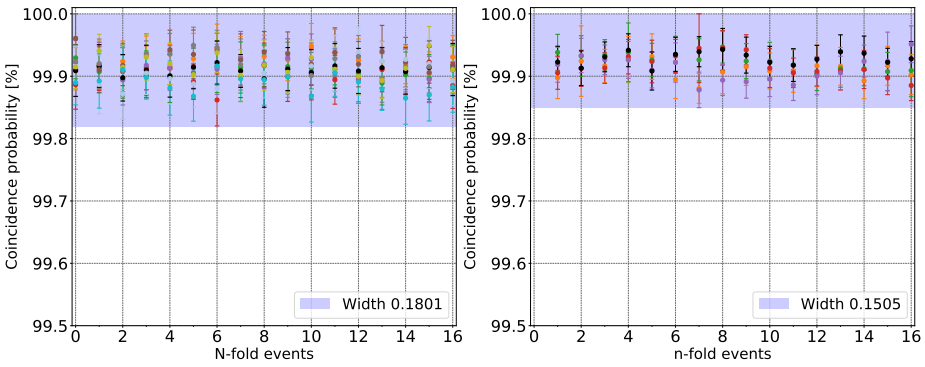

(a) Coincidence window 3 ns.

(b) Coincidence window 20 ns

Figure 4.7: The efficiency of high-order coincidences. Each colour symbolizes one configuration of the measurement.

Chapter 5

Measurement of optical states by means of multichannel single-photon detector

In this section, I present an analysis of the statistic of light. The states of light can be divided into classical, coherent, non-classical. One of the parameters characterizing light is probability distribution of the number of photons. Photon statistics plays an important role in many applications as quantum communication [35], quantum simulations [36], and non-classical light generation [37]. The photon statistics cannot be measured directly but can be reconstructed from click statistics. I use a photon number resolving detector and coincidence unit to get click statistics. From the click statistics, the state of the light can be classified using a binomial parameter. I show this method in the next section.

5.1 Probability distribution of coincidence events

The state of light can be characterized by criterion that allows to distinguish between classical and nonclassical behaviour such as the Wigner quasi-probability function [38] or Glauber distribution [39]. If we have a perfect photon number resolution detector, we can directly measure photon statistics. We can then use the Mandela parameter Q_M to classify the light. Mandel parameter is calculated as ratio of the mean value and variance of photon statistic. Traditional detectors emit photoelectron if a photon is absorbed. Emission probability is proportional to the intensity of the light. Because we don't have a perfect detector, we will use available binary detectors. The binary detectors click for any number of incoming photons and not click for a vacuum state. To achieve the photon number resolution, we use spatially multiplex and binary detectors (Figure 1.1). This detection systems provide click statistic. Therefore, we use the binomial parameter Q_b Introduced by Vogel [40]. The binomial parameter Q_b is directly constructed for measurements with photon number resolving detector (PNRD). The parameter Q_b is defined as:

$$Q_b = N\frac{\Delta^2 c}{\bar{c}(N-\bar{c})} - 1, \tag{5.1}$$

where $\bar{c}$ is the mean number, and $\Delta^2 c$ is the variance of clicks statistics. This statistical moments are defined as:

$$\bar{c} = \sum_{i=0}^{N} i c_i, \qquad \Delta^2 c = \sum_{i=0}^{N} (i-\bar{c})^2 c_i \tag{5.2}$$

One can see that click statistics converge to a true photon statistic with an increasing number of detectors. States of the light can be classified by Q_b values. The non-negative values of the Q_b parameter stand for classical states. The coherent state has $Q_b = 0$, and negative Q_b implies nonclassical states.

5.2 Experimental setup

Now, we show the usefulness of the coincidence unit for an analysis of the prepared state of light. The general schema of an experiment is illustrated in Fig 5.1. Pulsed light is generated by gain-switched VCSEL diode (OPV314AT) driven by home-made electronic pulse generator (Pulser) with a repetition rate of 2 MHz and the pulse length of 1 ns. The VCSEL diode (LD) emits light at a central wavelength of 810 nm. The optical signal is led over an optical attenuator (att) (a series of ND filters) to a photon number resolving detector (PNRD). PNRD is created by spatially multiplexed detectors [41]. The multiplexing approach is based on splitting an input optical signal by a set of beam splitters. The multiplexed optical signal is led to multiple binary detectors SPADs (Excelitas, type SPCM). Electrical outputs of multiplexed detectors are processed by presented coincidence unit. The coincidence windows are set to 20 ns. The coincidence events are accumulated into a histogram, which gives directly the click statistics.

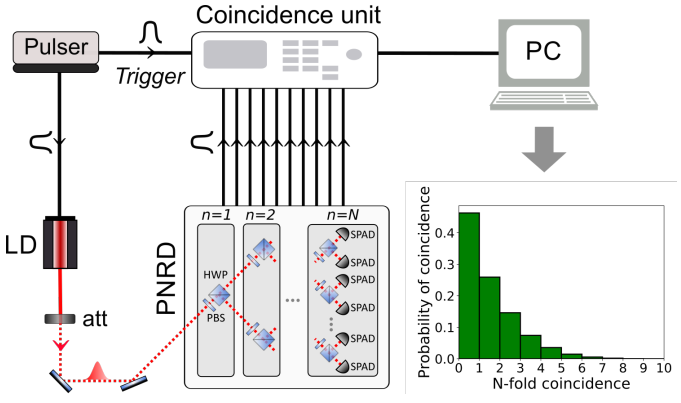

Figure 5.1: Experimental setup for analysis of unknown optical states by measuring statistics clicks. The optical signal is lead to the PNRD detector. The output of the PNRD is processed by a coincidence unit. The coincidence unit accumulates the coincidences events and evaluates the click statistics.

We measured coherent and thermal states with several different mean numbers of photons. The click statistics for two particular states are depicted in Figure 5.2,5.3. The first and the second moment of the probability distribution of the coincidence events are necessary for the calculation of the binomial parameter. The statistical moments are calculated from raw click statistics. The Q_b (5.1) parameter for all states with errorbars is reported in Fig 5.4.

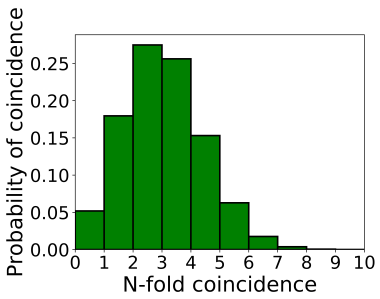

Figure 5.2: The click statistics of a coherent state. This state has mean value $\bar{c} = 2.64(3)$ and variance $\Delta^2 c = 1.906(7)$.

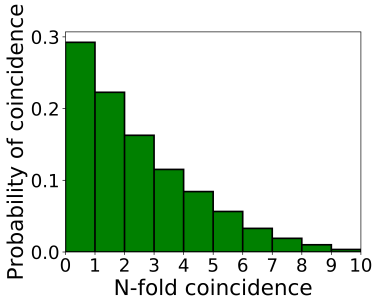

Figure 5.3: The click statistics of a thermal state. This state has means value $\bar{c} = 1.95(2)$ and variance $\Delta^2 c = 3.91(4)$.

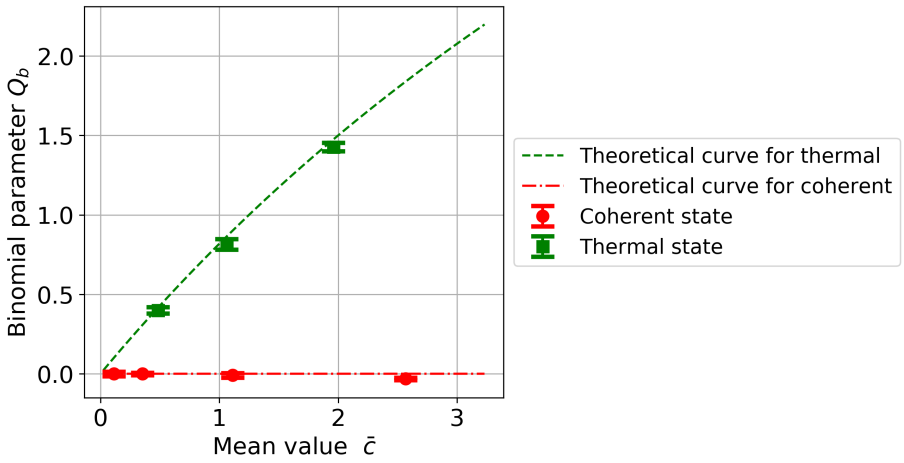

Figure 5.4: The Q_b parameters for the coherent (red) and thermal (green) state with mean number $\bar{c}$. The graph also contains a theoretical curves that describe the general behavior of these states.

Our results show that binomical parameter for coherent states has a mean

value of about zero, which corresponds with the theory. The second tested class was a thermal state that represents a classical light. All measured thermal states, within the errorbar, lie on the theoretical curve (Fig.5.4). This results show that the value of Q_b parameters allows the classify state of light. These results were achieved with 10 detectors, where the average error of Q_b parameter is 10^{-3}. If we increase the number of detectors, we also reduced the measurement error. A higher number of detectors also makes it possible to measure states with a higher mean value i.z. the dynamic range increases. We plan to build a multi-channel detector with more that 30 channels.

Chapter 6

Conclusion

In this work, I dealt with the detection and processing of the weak optical signal at the single-photon level. For the detection of a photon, I used a single-photon detector based on avalanche photodiode SAP500 manufactured by Laser Components. For this diode, I build a passive quenching circuit. I first dealt with signal processing from this home-built SPAD. In general, the output signal from SPAD does not have a constant level of amplitude. I solved the problem of how to record the signal from SPAD and we created a procedure for correct signal recording. I also characterized parameters of the SPAD as dark count and detection efficiency. I measured the dependence of these parameters on temperature and overvoltage. From our measurements, we found that the DC rate increases with temperature and overvoltage.

Another measured parameter was relative detection efficiency. For this measurement, I used a reference detector with absolute detection efficiency of about 66%. I measure the same optical signal with both detectors and from this measurement, I recalculate detection efficiency for our detector. For 20 V of overvoltage and T=0 $^{\circ}C$ the detection efficiency of SAP500 approaches the reference commercial SPAD.

The last I measure a dead time, which is given mainly by the used quenching circuit. I found that the dead time is not constant but fluctuates with overvoltage. For overvoltage 20 V the dead time is 630(30) ns which is comparable to a commercial passively quenching detector.

In section 4 I present the fast multichannel coincidence counting unit. I perform a detailed characterization of its parameters. To control the CCU I wrote and optimized a library of commands. I found that coincidence windows are almost perfect rectangles, because the rising edge of the window has an average length of 15(3) ps, and the average value of the falling edge is 22(9) ns. The best achievable edges have length only 7.1(3) ns.

I also examined the efficiency of high-order coincidences. I measured 16 coincidence for different width of coincidence windows and I try different combinations of the gradual switch of channels. The result shows that differences between individual order of coincidence are 0.18% for 3 ns coincidence windows and 0.15 % for 20 ns coincidence windows. This shows that the coincidence unit has good efficiency of high-order coincidences.

Chapter 5 presented the use of a coincidence unit for click statistics analysis. We measured several different mean numbers of photons of coherent and thermal

state. Using the Q_b parameter, we evaluated the light non-classicality. Our results show that all states correspond to theoretical values. These results were achieved with 10 detectors, where the average error of Q_b parameter is 10^{-3}.

We will continue to work on the development of a new version of the coincidence unit that eliminates imperfection describe in chaplet 4. We also want to expand the number of channels of coincidence unit up to 30. For this coincidence unit, we want to build an adjustable multichannel detector based on the avalanche diode. We used the results from chapter 3 to construct a multichannel detector with more than 30 channels.

Bibliography

[1] A. R. Dixon, Z. L. Yuan, J. F. Dynes, A. W. Sharpe, and A. J. Shields, "Gigahertz decoy quantum key distribution with 1 mbit/s secure key rate," *Opt. Express*, vol. 16, pp. 18790–18797, Nov 2008.

[2] A. Kufcsák, A. Erdogan, R. Walker, K. Ehrlich, M. Tanner, A. Megia-Fernandez, E. Scholefield, P. Emanuel, K. Dhaliwal, M. Bradley, R. K. Henderson, and N. Krstajić, "Time-resolved spectroscopy at 19,000 lines per second using a cmos spad line array enables advanced biophotonics applications," *Opt. Express*, vol. 25, pp. 11103–11123, May 2017.

[3] J. G. Rarity, P. Owens, and P. Tapster, "Quantum random-number generation and key sharing," *Journal of Modern Optics*, vol. 41, no. 12, pp. 2435–2444, 1994.

[4] A. Stefanov, N. Gisin, O. Guinnard, L. Guinnard, and H. Zbinden, "Optical quantum random number generator," *Journal of Modern Optics*, vol. 47, no. 4, pp. 595–598, 2000.

[5] R. H. Hadfield, "Single-photon detectors for optical quantum information applications," *Nature photonics*, vol. 3, no. 12, p. 696, 2009.

[6] M. D. Eisaman, J. Fan, A. Migdall, and S. V. Polyakov, "Invited review article: Single-photon sources and detectors," *Review of scientific instruments*, vol. 82, no. 7, p. 071101, 2011.

[7] P. Eckert, H.-C. Schultz-Coulon, W. Shen, R. Stamen, and A. Tadday, "Characterisation studies of silicon photomultipliers," *Nuclear Instruments and Methods in Physics Research Section A: Accelerators, Spectrometers, Detectors and Associated Equipment*, vol. 620, no. 2-3, pp. 217–226, 2010.

[8] A. Migdall, S. V. Polyakov, J. Fan, and J. C. Bienfang, *Single-photon generation and detection: physics and applications*. Academic Press, 2013.

[9] K. D. Irwin and G. C. Hilton, "Transition-edge sensors," in *Cryogenic particle detection*, pp. 63–150, Springer, 2005.

[10] G. Brida, M. Genovese, and I. R. Berchera, "Experimental realization of sub-shot-noise quantum imaging," *Nature Photonics*, vol. 4, no. 4, p. 227, 2010.

[11] V. Giovannetti, S. Lloyd, and L. Maccone, "Quantum metrology," *Physical review letters*, vol. 96, no. 1, p. 010401, 2006.

[12] T. Länger and G. Lenhart, "Standardization of quantum key distribution and the etsi standardization initiative isg-qkd," *New Journal of Physics*, vol. 11, no. 5, p. 055051, 2009.

[13] L.-M. Duan, M. D. Lukin, J. I. Cirac, and P. Zoller, "Long-distance quantum communication with atomic ensembles and linear optics," *Nature*, vol. 414, no. 6862, pp. 413–418, 2001.

[14] M. Genovese, "Research on hidden variable theories: A review of recent progresses," *Physics Reports*, vol. 413, no. 6, pp. 319–396, 2005.

[15] L. Mandel, "Quantum effects in one-photon and two-photon interference," in *More Things in Heaven and Earth*, pp. 460–473, Springer, 1999.

[16] J.-W. Pan, Z.-B. Chen, C.-Y. Lu, H. Weinfurter, A. Zeilinger, and M. Żukowski, "Multiphoton entanglement and interferometry," *Reviews of Modern Physics*, vol. 84, no. 2, p. 777, 2012.

[17] Y. Acremann, V. Chembrolu, J. Strachan, T. Tyliszczak, and J. Stöhr, "Software defined photon counting system for time resolved x-ray experiments," *Review of scientific instruments*, vol. 78, no. 1, p. 014702, 2007.

[18] S. Felekyan, R. Kühnemuth, V. Kudryavtsev, C. Sandhagen, W. Becker, and C. Seidel, "Full correlation from picoseconds to seconds by time-resolved and time-correlated single photon detection," *Review of scientific instruments*, vol. 76, no. 8, p. 083104, 2005.

[19] J. M. Senior and M. Y. Jamro, *Optical fiber communications: principles and practice*. Pearson Education, 2009.

[20] G. P. Agrawal, *Fiber-optic communication systems*, vol. 222. John Wiley & Sons, 2012.

[21] A. Gallivanoni, I. Rech, and M. Ghioni, "Progress in quenching circuits for single photon avalanche diodes," *IEEE Transactions on nuclear science*, vol. 57, no. 6, pp. 3815–3826, 2010.

[22] S. Cova, M. Ghioni, A. Lacaita, C. Samori, and F. Zappa, "Avalanche photodiodes and quenching circuits for single-photon detection," *Applied optics*, vol. 35, no. 12, pp. 1956–1976, 1996.

[23] S. Tisa, F. Zappa, A. Tosi, and S. Cova, "Electronics for single photon avalanche diode arrays," *Sensors and Actuators A: Physical*, vol. 140, no. 1, pp. 113–122, 2007.

[24] S. Cova, A. Longoni, and G. Ripamonti, "Active-quenching and gating circuits for single-photon avalanche diodes (spads)," *IEEE Transactions on nuclear science*, vol. 29, no. 1, pp. 599–601, 1982.

[25] C. Hu, T.-H. Ju, and Y. Yao, "Advantages and demonstration of gated-mode passive quenching with active reset circuit," in *2014 IEEE Workshop on Advanced Research and Technology in Industry Applications (WARTIA)*, pp. 953–956, IEEE, 2014.

[26] "swabianinstruments", ""time tagger user manual - swabian instruments"."

[27] B. Lounis and M. Orrit, "Single-photon sources," *Reports on Progress in Physics*, vol. 68, no. 5, p. 1129, 2005.

[28] M. Stipčević, B. G. Christensen, P. G. Kwiat, and D. J. Gauthier, "Advanced active quenching circuit for ultra-fast quantum cryptography," *Optics express*, vol. 25, no. 18, pp. 21861–21876, 2017.

[29] I. "Laser Components DG, ""sap500: Silicon apds for photon counting applications"."

[30] L. Neri, S. Tudisco, F. Musumeci, A. Scordino, G. Fallica, M. Mazzillo, and M. Zimbone, "Dead time of single photon avalanche diodes," *Nuclear Physics B-Proceedings Supplements*, vol. 215, no. 1, pp. 291–293, 2011.

[31] J. Grygar, *Jednofotonové lavinové detektory a jejich charakterizace*. PhD thesis, UP, 2018.

[32] P. Kok, W. Munro, K. Nemoto, T. Ralph, J. P. Dowling, and G. Milburn, "Publisher's note: Linear optical quantum computing with photonic qubits [rev. mod. phys. 79, 135 (2007)]," *Reviews of Modern Physics*, vol. 79, no. 2, p. 797, 2007.

[33] E. Knill, R. Laflamme, and G. J. Milburn, "A scheme for efficient quantum computation with linear optics," *nature*, vol. 409, no. 6816, pp. 46–52, 2001.

[34] M. Tillmann, B. Dakić, R. Heilmann, S. Nolte, A. Szameit, and P. Walther, "Experimental boson sampling," *Nature Photonics*, vol. 7, p. 540–544, May 2013.

[35] J. Dynes, M. Lucamarini, K. Patel, A. Sharpe, M. Ward, Z. Yuan, and A. Shields, "Testing the photon-number statistics of a quantum key distribution light source," *Optics express*, vol. 26, no. 18, pp. 22733–22749, 2018.

[36] M. D. Vidrighin, O. Dahlsten, M. Barbieri, M. Kim, V. Vedral, and I. A. Walmsley, "Photonic maxwell's demon," *Physical review letters*, vol. 116, no. 5, p. 050401, 2016.

[37] I. Straka, L. Lachman, J. Hloušek, M. Miková, M. Mičuda, M. Ježek, and R. Filip, "Quantum non-gaussian multiphoton light," *npj Quantum Information*, vol. 4, no. 1, pp. 1–5, 2018.

[38] E. Wigner, "On the quantum correction for thermodynamic equilibrium," *Phys. Rev.*, vol. 40, pp. 749–759, Jun 1932.

[39] R. J. Glauber, "Photon correlations," *Phys. Rev. Lett.*, vol. 10, pp. 84–86, Feb 1963.

[40] J. Sperling, W. Vogel, and G. Agarwal, "Sub-binomial light," *Physical review letters*, vol. 109, no. 9, p. 093601, 2012.

[41] J. Hloušek, M. Dudka, I. Straka, and M. Ježek, "Accurate detection of arbitrary photon statistics," *Physical review letters*, vol. 123, no. 15, p. 153604, 2019.

Chapter 7

Appendix A

The command of MCU firmware:

get_temp *(unit)*

- The function returns the actual temperature on the board.
- Parameters
  - unit (int) - Physical number of board (0-7)

get_volt *(unit)*

- The function returns the actual voltage on the board.
- Parameters
  - unit (int) - Physical number of board (0-7)

get_wtemp *()*

- The function returns the actual temperature on the main board.

set_wdac *(voltage)*

- The function sets a threshold for a trigger.
- Parameters
  - voltage (float) - Voltage from range -1 to 4 V.

set_wdel *(width, delay1, delay0)*

- The function sets the width and position of the trigger windows. The delay1 sets the position of a trigger. The Sum of Width and delay1 must be smaller than 9216 ps.

- Parameters
  - delay0 (int) - Delay time in picoseconds from range 0-9216.
  - delay1 (int) - Next delay time in picoseconds from range 0-9216.
  - width (int) - Time in picoseconds from range 0-9216.

set_dac *(channel, voltage)*

- The function sets a threshold for a channel.
- Parameters
  - Channel (int) - Physical channel number (0-15)
  - Voltage (float) - Voltage from range -1 to 4 V.

set_del *(channel, width, delay)*

- The function sets the width and position of the channel window. The Sum of Width and delay must be smaller than 9216 ps.
- Parameters
  - channel (int) - Physical channel number (0-15)
  - width (int) - Time in picoseconds from range 0-9216.
  - delay (int) - Delay time in picoseconds from range 0-9216.

start *(type)*

- The function begins a measurement.
- Parameters
  - type (int) - The switch sets the type of recording histogram.
    - 0 - Full histogram
    - 1 - Reduced histogram.

result *(type)*

- The function ends the measurement and sent data to the buffer.
- Parameters
  - type (int) - The switch sets the type of recording histogram.
    - 0 - Full histogram
    - 1 - Reduced histogram.

Chapter 8

Appendix B

The commands of CCU python library.

Commands library

clear()

- The function removes all symbols from the buffer. The function is used after errors and after incomplete measurement.

recording(*name, type, mtime ,regime*)

- The function measures the coincidence event.
- Parameters
  - mtime (float) - Time of measurement.
  - name (sting) - Name of file.
  - type (int) - The switch sets the type of recording histogram
    - 0 - Full histogram
    - 1 - Reduced histogram
  - regime (int) - Switch specifying data storage
    - 0 - Data are save as .TXT file
    - 1 - Data stay in PC memory

display_single(*channel, repetition, mtime*)

- The function displays singles.
- Parameters
  - channel (int) - Physical channel number (0-15)
  - repetition(int) - Number of measurement repetitions
  - mtime (float) - Time of individual measurement.

calibration(*channel, mtime, w_channel ,w_trigr, trigr_del, volt_ch, volt_trigger, name*)

- The function measures the total length of the coincidence window for singles. The function used scanning (Chap. **??**). Function returns txt file with the coincidence numbers for the given step.
- Parameters
  - channel (int) - Physical channel number (0-15)
  - mtime (float) - Measurement time of one step delay line
  - w_channel (int) - Width of channel in picoseconds from range 0-9216
  - w_trigr (int) - Width of trigger in picoseconds from range 0-9216
  - trigr_del (int) - Delay of trigger in picoseconds from range 0-9216
  - volt_ch (float) - Threshold for a channel
  - volt_trigger (float) - Threshold for a trigger
  - name (sting) - Name of file

fast_calibration(*channel_list, mtime, w_channel ,w_trigr, trigr_del, volt_ch, volt_trigger, name*)

- This function does a scan of the rising and falling edges. This function is faster than function Calibration. The Function returns the file with the coincidence numbers for the given step.
- Parameters
  - channel (list) - List of channels
  - mtime (float) - Measurement time of one step delay line
  - w_channel (int) - Width of channel in picoseconds from range 0-9216
  - w_trigr (int) - Width of trigger in picoseconds from range 0-9216
  - trigr_del (int) - Delay of trigger in picoseconds from range 0-9216.
  - volt_ch (float) - Threshold for a channel
  - volt_trigger (float) - Threshold for a trigger
  - name (sting) - Name of file

Scan_channel(*channel, mtime, w_channel ,w_trigr, trigr_del, volt_ch, volt_trigger*)

- The function served for a set external delay and show the position of channel windows. Function print numbers of singles for a selected channel on screen.
- Parameters
  - channel (int) - Physical channel number (0-15)

- mtime (float) - Measurement time of one step delay line
- w_channel (int) - Width of channel in picoseconds from range 0-9216
- w_trigr (int) - Width of trigger in picoseconds from range 0-9216
- trigr_del (int) - delay of trigger in picoseconds from range 0-9216.
- volt_ch (float) - Threshold for a channel
- volt_trigger (float) - Threshold for a trigger

Set_width(*channel_list, m_time, w_channel ,w_trigger, trigger_del, volt_channel, volt_trigger, w_want, name*)

- This function is used for setting a real width and alignment of coincidence windows. All channels from the channel list are scanned by function fast_calibration(). The width of coincidence windows is compared with the required width (w_want). Channel with different width is stretch or shorten. This process is iterative. Function save the file with parameters about and alignment and set the width.
- Parameters
  - channel (list) - List of channels
  - mtime (float) - Measurement time of one step delay line
  - w_channel (int) - Width of channel in picoseconds from range 0-9216
  - w_trigr (int) - Width of trigger in picoseconds from range 0-9216
  - trigr_del (int) - dDelay of trigger in picoseconds from range 0-9216.
  - volt_channel (float) - Threshold for a channel
  - volt_trigger (float) - Threshold for a trigger
  - w_want (float) - Required width of coincidence windows
  - name (string) - Name of file